A Simple Design Approach for an Electro-Hydraulic Stewart Platform Through Matlab Simulation

Anirban Bose
Assistant Professor, Mechanical Engg. Dept.
Meghnad Saha Institute of Technology
Kolkata, India
a.bose@rediffmail.com

Rana Saha
Assistant Professor, Mechanical Engg. Dept.
Jadavpur University
Kolkata, India
rsaha@mech.jdvu.ac.in

Kamalesh Majumdar
Professor, Mechanical Engg. Dept.
Jadavpur University
Kolkata, India
kamalesh_majumdar@hotmail.com

Dipankar Sanyal
Professor, Mechanical Engg. Dept.
Jadavpur University
Kolkata, India
dsanyal@mech.jdvu.ac.in

***Abstract*— A Stewart platform has been designed by selecting commercially available components. Each of its six legs has spherical and universal joints respectively at the bottom and top ends of a piston-cylinder arrangement with the piston rod protruding out of the cylinder top. By a universal joint at the cap end at the bottom of each cylinder, the legs are mounted on a fixed horizontal frame. By electrical actuation of the valve for each cylinder, a six-DOF motion could be imparted to a cylindrical payload fixed on a circular disc. The motion is transferred through a spherical joint fitted between each piston rod and the disc. Corresponding to the specified payload pose range from its horizontal neutral, the inverse kinematic model has been used for simultaneously searching the piston stroke, the distance between the frame and the disc along with the locations of the joints, assuming each type arranged in a semi-regular hexagonal pattern. The discharge and pressure of a power pack feeding all the cylinders have been estimated by Matlab simulation of the inverse dynamic model for different velocity, acceleration and weight of the payload.**

Keywords—Inverse model, kinematics, dynamics, Six-DOF motion

I. INTRODUCTION

A Stewart platform [1] is the most popular parallel manipulator with six degrees-of-freedom widely used as laboratory-scale flight or ship-motion simulators. It involves six linearly extensible legs with active electric or hydraulic drive for each. In a conventional Stewart platform, the bottom end of each leg is connected by a spherical or universal joint to a stationary frame at the bottom and the top end is connected by a spherical joint to the moving platform that supports a payload on top. Legs only with prismatic joints between its upper and lower parts have been analyzed in the past, though nowadays various laboratories are exploring the use of ball-screw joints [2]. Both 6-SPS and 6-UPS configurations have been extensively analyzed [3-6], where 6 stands for the number of joints of same type, the first alphabet S or U corresponds to spherical or universal joint with the fixed frame at one end of each leg, P refers to the prismatic joint within each leg and the last alphabet S implies spherical joint with the moving platform at the other end.

Joints at the bottom and at the top are usually arranged along the vertices of two regular [4] or semi-regular hexagons [3, 5]. Merlet [4] considered 3/6 configuration, in which one of the ends of two legs terminated to a common bi-spherical joint, each located at the vertex of an equilateral triangle. Controlling the input to each leg is necessary, causing its length to change, with the objective of carrying the top platform through desired position and orientation, together called the pose. Liu et al. [3] and Merlet [4] modeled both the forward and inverse kinematics of a Stewart platform and proposed simplified solution schemes for the forward kinematics. In particular, the inverse kinematics deals with estimating the neutral length and stroke of the legs from the specified range of desired platform pose. Employing Newton-Eulerian analysis, Dasgupta and Mrithyunjaya [5, 6] arrived at both inverse and forward models for the kinematics and dynamics. The inverse dynamics model enables determination of actuation force or torque that should be imparted to the payload in order to achieve its desired range of motions.

Though electro-hydraulic actuation has been extensively used in many Stewart platform investigations [7-10], only a few of those deal with the pressure-discharge relations of valve and cylinder under electrical actuation of the valve. For instance, Huang et al. [7] and Huang and Fu [8] verified the performance of their proposed sliding-mode control in an experimental set up that has electro-hydraulic valves and cylinders. But, the hydraulic details in the control model were not explicitly dealt with, depending on the sliding-mode control for its capability of dealing with uncertainties. On the other hand, Li and Salcudean [9] and Davliakos and Papadopoulos [10] considered the electro-hydraulic aspects in their control analysis involving the forward kinematic and dynamic modeling of the system. Friction force between the piston and the cylinder that is the chief source of nonlinearity in hydraulic systems has been modeled in the latter study. Although, they considered the viscous friction and Coulomb friction, Stribeck effect [11] that imparts the well-known non-monotonic character to the variation of friction force and piston velocity was neglected.

The design of a Stewart platform driven by variable-speed DC motor actuated legs with ball-screw joint has been recently undertaken by Halder et al. [2]. Though most of the existing literature deals with either experiment or control design, very few of them deal with the design. A design procedure for an electro-hydraulically actuated Stewart platform driven has been reported here. The design has been accomplished by using the inverse kinematic and dynamic modeling of the system along with detailed electro-hydraulic model. While commercially available components like six sets of universal joints, spherical joints, hydraulic piston and cylinder arrangements and proportional valves along with a hydraulic power pack have been selected.

It may be mentioned here that the existing body of research has grossly overlooked the design aspect of the problem. A simultaneous nested search has been executed in this study for given payload size and range of its demanded pose and the rates, along with the constraints of the permissible maximum joint angles and available actuation capabilities. The design has been accomplished by implementing the inverse kinematic and dynamic models in Matlab.

II. System Configuration

Figure 1 shows the schematic of a electro-hydraulically actuated Stewart platform with a fixed semi-regular hexagonal frame $b^1b^2b^3b^4b^5b^6$ on the ground and a circular disc $t^1t^2t^3t^4t^5t^6$ on top connected by six extensible legs. Each leg has a universal joint with the bottom frame, a spherical joint with the top disc and a hydraulic cylinder with a piston between these joints. While a universal joint is shown by a filled circle, an empty circle represents a spherical joint. Each cylinder has been shown to be asymmetric with the piston rod protruding out of it only at the top. Along with each cylinder, a corresponding four-port proportional valve for controlling the piston motion has been represented in the figure symbolically. There is a common hydraulic power pack with a pump, a pressure-relief valve and a reservoir, all represented by their usual symbols. Though the symbol of the reservoir has been used in several places, they stand for the same reservoir. An integer between 1 to 6, either at the subscript or the superscript, has been used for the different variables and the geometric descriptions pertaining to each of the six legs, which has also been described in the text in a general manner by using *i* instead of the integer.

A universal joint i with center at B^i supports the cap-

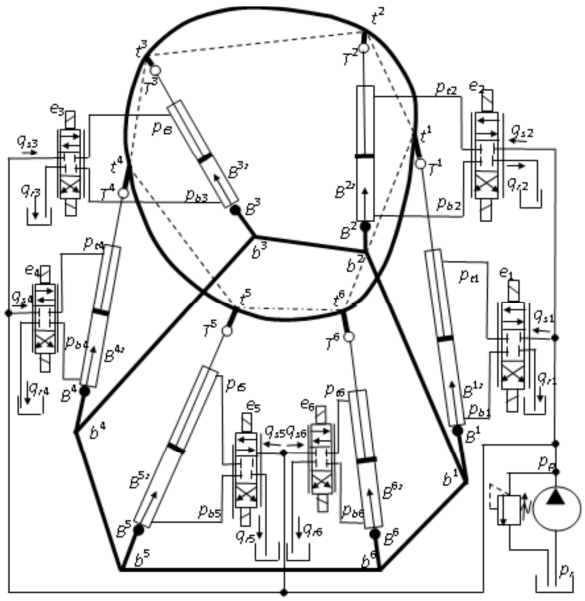

Fig. 1. Schematic of an electro-hydraulic Stewart platform

end of the i^{th} cylinder on the bottom frame through one arm b^iB^i of the joint. The supply and return discharges through the i^{th} valve are q_{si} and q_{ri} respectively, which could reach to one end of the cylinder and comes back from the other end. Not only these discharges, but also the pressures p_{ti} and p_{bi} at the top and bottom chamber of the cylinder are controlled by the respective electrical command signal e_i each valve. The difference of pressure within the cylinder across the piston causes the piston to reciprocate relative to the cylinder.

In the system depicted in Figure 1, six DOF motion could be imparted to the top disc through the spherical joints with centers at T^i. The top platform is a circular disc supported on the universal joints at the points t^i, where T^it^i is the top arm of the i^{th} joint. The joints together comprise four semi-regular hexagons $t^1t^2t^3t^4t^5t^6$, $T^1T^2T^3T^4T^5T^6$, $B^1B^2B^3B^4B^5B^6$ and $b^1b^2b^3b^4b^5b^6$ with circum radii equal to r_t , r_T, r_B or r_b respectively. For the ease of analysis, the disc and a cylindrical payload that would be supported on it has been assumed to be coaxial and for the simplicity of the presentation only the rim of the top disc has been shown. Figure 2 that has been employed to describe the inverse modeling of the entire system shows the payload explicitly.

III. INVERSE KINEMATIC MODELING

Different coordinate systems used in this study for the 6-DOF motion analysis of the payload are a stationary global Cartesian coordinate system (x, y, z) with its origin at O, a payload-fitted moving coordinate system ($p^x(t)$, $p^y(t)$, $p^z(t)$) attached to the center of mass at p for the combined payload and the disc that moves in space and six rotating coordinate systems ($B^{ix}(t)$, $B^{iy}(t)$, $B^{iz}(t)$) attached to the stationary points B^i. The origins of all these coordinate systems have been indicated in Figure 2. It depicts the payload and the disc along with their poses at neutral (0,0,0,0,0,0) and at another pose (x,y,z,0,0,θ_z). For both the poses, the leg configurations have also been indicated in the bottom part of the figure. In the top part only the disc and the payload have been shown along with different axes. Solid lines and dashed lines indicate the details of the arrangement respectively at the neutral and away from it. Chain-dashed lines have been used to mark the axes in the figure. Like Figure 1, the filled and empty circles represent the centers of the universal and the spherical joints respectively. Only the top of the disc and the axes of the piston-cylinder pairs have been shown.

The displacements x, y and z are referred as surge (Su), sway (Sw) and heave (H) respectively, while the angular displacements θ_x, θ_y and θ_z are called roll (R), pitch (P) and yaw (Y) respectively that together has been referred as SuSwHRPY. It is customary to specify the three angular displacements in the said order. A look at Figure 2 would make it evident that if the payload executes the yawing motion once the payload axis and p reach their respective desired orientation and position away from the neutral, the disc would require to slip at some joint of each of the actuation system about a vertical axis. Otherwise, a large stress would develop in the system. In order to overcome this problem, at the top end of each actuation system, a spherical joint has been selected.

For the clarity of the presentation, a pose of the payload has been shown in Figure 2 with positive surge, sway, heave and yaw, but no roll and pitch. The neutral position is achieved, when the axes of the cylinder and its end joints B^iT^i, b^iB^i and t^iT^i respectively are collinear. This collinear setting and the departure from it in a position other than the neutral are apparent from the figure. With respect to the designation at the neutral, an additional / has been used to indicate various points and axes in the position away from the neutral. Only for the payload-fixed coordinate system, its dependence on time t has been explicitly mentioned.

Along with the stationary global coordinate system with axes Ox, Oy and Oz, the payload-fixed moving coordinate system has been shown with axes px, py and pz at the neutral pose and $p'p^x(t)$, $p'p^y(t)$, and $p'p^z(t)$ for the pose away from the neutral. While the fixed origins of the rotating coordinate system at B^i have been shown in both Figures 1 and 2, the directions along the cylinder axis B^{iz} have been indicated only in Figure 1. Each of the i^{th} cylinder could have a passive rotation about the axis B^{iz} along with an active rotation in which the axis B^{iz} rotates about a horizontal axis passing through B^i. While the active rotation contributes to the payload motion, by allowing the passive rotation the internal stresses of the actuation system is contained. The rotating coordinate system is chosen in a manner such that at any instant of time, the active motion of a piston remains fully contained in the plane $B^{iz}B^{ix}$. Obviously, the axes B^{ix} and B^{iy} are connected to the specific demand of the payload motion. Therefore, these have not been explicitly shown in the figures.

An objective of the inverse kinematic modeling is to express the instantaneous variations of the stroke of the pistons in terms of the instantaneous variation of the desired pose. These can be determined through the pertinent expressions for coordinates of the end points B^i and T^i of each leg. Thus, it is necessary to represent the variables related to the pose for different points associated with the legs. In terms of the scalar components indicated by the italicized variables, the bold-faced symbols that have been used for the different vectors are

$$\mathrm{x} = (x \quad y \quad z)^T \tag{1a}$$

$$\mathbf{v} = (v_x \quad v_y \quad v_z)^T \tag{1b}$$

$$\mathbf{a} = (a_x \quad a_y \quad a_z)^T \tag{1c}$$

$$\boldsymbol{\theta} = (\theta_{p^x} \quad \theta_{p^y} \quad \theta_{p^z})^T \tag{1d}$$

$$\boldsymbol{\omega} = (\omega_{p^x} \quad \omega_{p^y} \quad \omega_{p^z})^T \tag{1e}$$

$$\boldsymbol{\alpha} = (\alpha_{p^x} \quad \alpha_{p^y} \quad \alpha_{p^z})^T \tag{1f}$$

for the linear displacement, velocity and acceleration and the angular displacement, velocity and acceleration of the payload respectively with the subscript to scalar components indicating the coordinate direction. In the customary manner, the linear and angular variables for the platform have been represented in the stationary and the payload-fixed coordinate systems respectively.

It is evident that the payload displacement has been taken to be equal to the displacement of the mass center p. With respect to this displacement, each of the positions of p, q and o has the additional component of the corresponding vertical height at the neutral above or below O. Using a subscript inside parentheses to indicate a variable at a point, therefore, it may be written that

$$\mathbf{x}_{(p)} = x\hat{i} + y\hat{j} + (z + z^0_{(p)})\hat{k} \tag{2a}$$

$$\mathbf{x}_{(q)} = x\hat{i} + y\hat{j} + (z + z^0_{(q)})\hat{k} \tag{2b}$$

$$\mathbf{x}_{(Q)} = x\hat{i} + y\hat{j} + (z + z^0_{(Q)})\hat{k} \tag{2c}$$

where the superscript 0 indicates the variable at the neutral position. It is apparent from the figure that the bottom ends of the actuators at B^1, B^2, B^3, B^4, B^5 and B^6 are fixed in space, while the top ends at T^1, T^2, T^3, T^4, T^5 and T^6 move with the payload. Though the figure shows only

the radius r_t of the circle through all t^i from the center q that is independent of the platform pose, radius r_T of the circle through all T^i from the center at Q is also independent of the platform pose. Since b^i and B^i do not move, the radius r_B of the circle through all B^i from the center at O and the radius r_b of the circle through all b^i from the center at o are also fixed. Clearly, the coordinates of B^i, b^i, t^i and T^i are

$$\mathbf{x}_{(Bi)}=(r_B\cos\theta_{(Bi)} \quad r_B\sin\theta_{(Bi)} \quad 0)^T \tag{3a}$$

$$\mathbf{x}_{(bi)}=(r_b\cos\theta_{(bi)} \quad r_B\sin\theta_{(bi)} \quad z_{(bi)})^T \tag{3b}$$

$$\mathbf{x}_{(ti)}=\mathbf{x}_{(q)}+\mathbf{r}_{\mathbf{O}(ti),(q)} \tag{3c}$$

$$\mathbf{x}_{(Ti)}=\mathbf{x}_{(Q)}+\mathbf{r}_{\mathbf{O}(Ti),(Q)} \tag{3d}$$

where the symbol $\mathbf{r}_{\mathbf{c}(a),\,(b)}$ represents the position vector of a with respect to b in the coordinate system with origin at c yielding

$$\mathbf{r}_{\mathbf{O}(ti),(q)}=\mathbf{R}^T_{p,o}(r_t\cos\theta_{(ti)} \quad r_t\sin\theta_{(ti)} \quad z^0_{(q)}-z^0_{(p)})^T \tag{3e}$$

$$\mathbf{r}_{\mathbf{O}(Ti),(Q)}=\mathbf{R}^T_{p,o}(r_T\cos\theta_{(Ti)} \quad r_T\sin\theta_{(Ti)} \quad z^0_{(Q)}-z^0_{(p)})^T \tag{3f}$$

with various angles appearing in Equations (3a), (3b), (3e) and (3f) can be expressed in terms of the angle θ_s shown in Figure 2 as

$$\theta_{(t1)}=-\theta_s,\ \theta_{(t2)}=\theta_s,\ \theta_{(ti)}=\theta_{(t,i-2)}+2\pi/3,\ i=3\text{ to }6 \tag{4a}$$

$$\theta_{(b1)}=\theta_s-(\pi/3),\ \theta_{(b2)}=(\pi/3)-\theta_s,\quad \theta_{(bi)}=\theta_{(b,i-2)}+2\pi/3,\ i=3\text{ to }6 \tag{4b}$$

$$\theta_{(Ti)}=\theta_{(ti)}+(\theta_{(bi)}-\theta_{(ti)})z^0_{(Q)}/z^0_{(q)},\quad i=1\text{ to }6 \tag{4c}$$

$$\theta_{(Bi)}=\theta_{(bi)}-(\theta_{(bi)}-\theta^0_{(ti)})z_{(O)}/z^0_{(q)},\quad i=1\text{ to }6 \tag{4d}$$

and in Equations (3e) and (3f), the rotation matrix for transforming a vector from the moving to stationary coordinate system is

$$\mathbf{R}_{p,o}=(\mathbf{i}^T_{p\mathbf{x}} \quad \mathbf{j}^T_{p\mathbf{x}} \quad \mathbf{k}^T_{p\mathbf{x}})^T \tag{5a}$$

where

$$\mathbf{i}^T_{p\mathbf{x}}=(\mathrm{c}\theta_y\mathrm{c}\theta_z \quad \mathrm{s}\theta_x\mathrm{s}\theta_y\mathrm{c}\theta_z+\mathrm{c}\theta_x\mathrm{s}\theta_z \quad -\mathrm{c}\theta_x\mathrm{s}\theta_y\mathrm{c}\theta_z+\mathrm{s}\theta_x\mathrm{s}\theta_z) \tag{5b}$$

$$\mathbf{j}^T_{p\mathbf{x}}=(-\mathrm{c}\theta_y\mathrm{s}\theta_z \quad -\mathrm{s}\theta_x\mathrm{s}\theta_y\mathrm{s}\theta_z+\mathrm{c}\theta_x\mathrm{c}\theta_z \quad -\mathrm{c}\theta_x\mathrm{s}\theta_y\mathrm{s}\theta_z+\mathrm{s}\theta_x\mathrm{c}\theta_z) \tag{5c}$$

$$\mathbf{k}^T_{p\mathbf{x}}=(\mathrm{s}\theta_y \quad -\mathrm{s}\theta_x\mathrm{c}\theta_y \quad \mathrm{c}\theta_x\mathrm{c}\theta_y) \tag{5d}$$

Where

$\mathrm{c}\alpha=\cos\alpha$ and $\mathrm{s}\alpha=\sin\alpha$

The fixed lengths of the top arm of the i^{th} spherical joint, the bottom stubs and the bottom arm of the i^{th} universal joint, the instantaneous length of the i^{th} leg along with the angles between the two arms in the top and bottom joints cab be expressed respectively as

$$l_{Ti}=\left|\mathrm{x}_{(ti)}-\mathrm{x}_{(Ti)}\right| \tag{6a}$$

$$l_{Bi}=\left|\mathbf{x}_{(Bi)}-\mathbf{x}_{(bi)}\right| \tag{6b}$$

$$l_{ai}=\left|\mathbf{x}_{(Ti)}-\mathbf{x}_{(Bi)}\right| \tag{6c}$$

$$\alpha_{Ti}=\cos^{-1}(\hat{\mathbf{e}}_{tTi}.\hat{k}_{Bi}) \tag{6d}$$

$$\alpha_{Bi}=\cos^{-1}(\hat{\mathbf{e}}_{Bbi}.\hat{k}_{Bi}) \tag{6e}$$

Where

$$\hat{\mathrm{e}}_{tTi}=(\mathbf{x}_{(ti)}-\mathbf{x}_{(Ti)})/\left|\mathbf{x}_{(ti)}-\mathbf{x}_{(Ti)}\right| \tag{6f}$$

$$\hat{\mathrm{e}}_{Bbi}=(\mathbf{x}_{(Bi)}-\mathbf{x}_{(bi)})/\left|\mathbf{x}_{(Bi)}-\mathbf{x}_{(bi)}\right| \tag{6g}$$

and in Equations (6d) and (6e) $\hat{k}_{Bi}$ belongs to the unit vector set in i^{th} rotating coordinate system expressed as

$$\hat{\mathbf{e}}_{Bi}=(\hat{i}_{Bi} \quad \hat{j}_{Bi} \quad \hat{k}_{Bi})^T=\mathbf{R}_{Bi,o}(\hat{i} \quad \hat{j} \quad \hat{k})^T \tag{7a}$$

where (a) the unit vector along B^{iz} direction given by

$$\hat{k}_{Bi}=(\mathbf{x}_{Ti}-\mathbf{x}_{Bi})/\left|\mathbf{x}_{Ti}-\mathbf{x}_{Bi}\right|=k_{Bix}\hat{i}+k_{Biy}\hat{j}+k_{Biz}\hat{k}=\mathbf{k}^T_{Bi\mathbf{x}}\hat{\mathbf{e}} \tag{7b}$$

(b) the unit vector along B^{iy} direction in case the payload is in motion or stationary given respectively by

$$\hat{j}_{Bi}=(\mathbf{x}_{Ti}-\mathbf{x}_{Bi})\times\mathbf{v}_{Ti}/\left|(\mathbf{x}_{Ti}-\mathbf{x}_{Bi})\times\mathbf{v}_{Ti}\right|=j_{Bix}\hat{i}+j_{Biy}\hat{j}+j_{Biz}\hat{k}=\mathbf{j}^T_{Bi\mathbf{x}}\hat{\mathbf{e}} \tag{7c}$$

or

$$\hat{j}_{Bi}=\mathbf{r}_{Ti,Bi}\times\mathbf{v}_{Ti}/\left|\mathbf{r}_{Ti,Bi}\times\mathbf{v}_{Ti}\right|=j_{Bix}\hat{i}+j_{Biy}\hat{j}+j_{Biz}\hat{k}=\mathbf{j}^T_{Bi\mathbf{x}}\hat{\mathbf{e}} \tag{7d}$$

and (c) the unit vector along B^{ix} direction written as

$$\hat{i}_{Bi}=\hat{j}_{Bi}\times\hat{k}_{Bi}=i_{Bix}\hat{i}+i_{Biy}\hat{j}+i_{Biz}\hat{k}=\mathbf{i}^T_{Bi\mathbf{x}}\hat{\mathbf{e}} \tag{7e}$$

with the rotational matrix for transforming a vector from the i^{th} rotating to stationary coordinate system given as

$$\mathbf{R}_{Bi,o}=(\mathbf{i}^T_{Bi\mathbf{x}} \quad \mathbf{j}^T_{Bi\mathbf{x}} \quad \mathbf{k}^T_{Bi\mathbf{x}})^T \tag{7f}$$

where

$$\mathbf{i}^T_{Bi\mathbf{x}}=(j_{Biy}k_{Biz}-j_{Biz}k_{Biy} \quad j_{Biz}k_{Bix}-j_{Bix}k_{Biz} \quad j_{Bix}k_{Biy}-j_{Biy}k_{Bix}) \tag{7g}$$

$$\mathbf{j}^T_{Bi\mathbf{x}}=\begin{pmatrix}(y_{(Ti),(Bi)}v_{z(Ti)} & (z_{(Ti),(Bi)}v_{x(Ti)} & (x_{(Ti),(Bi)}v_{y(Ti)}\\ -z_{(Ti),(Bi)}v_{y(Ti)})/\Delta_{jBi} & -x_{(Ti),(Bi)}v_{z(Ti)})/\Delta_{jBi} & -y_{(Ti),(Bi)}v_{x(Ti)})/\Delta_{jBi}\end{pmatrix} \tag{7h}$$

$$\mathbf{k}^T_{Bi\mathbf{x}}=((x_{(Ti)}-x_{(Bi)})/l_{ai} \quad (y_{(Ti)}-y_{(Bi)})/l_{ai} \quad (z_{(Ti)}-z_{(Bi)})/l_{ai}) \tag{7i}$$

$$\Delta_{jBi}=[(y_{(Ti),(Bi)}v_{z(Ti)}-z_{(Ti),(Bi)}v_{y(Ti)})^2+(z_{(Ti),(Bi)}v_{x(Ti)}-x_{(Ti),(Bi)}v_{z(Ti)})^2+(x_{(Ti),(Bi)}v_{y(Ti)}-y_{(Ti),(Bi)}v_{x(Ti)})^2]^{1/2} \tag{7j}$$

There are physical constraints on the angles estimated by Equations (6d) and (6e), since the angle between the axes of two arms in relative motion in a joint should be within a limit depending on its design. Moreover, for each piston there is a permissible maximum stroke between the heads of the corresponding cylinder. Therefore, the length of the legs should be calculated from Equation (6c) for different poses within the specified range. The difference between the maximum and the minimum lengths thus

obtained should be restricted within the permissible stroke for the cylinder to be selected.

Besides the permissible joint angles and piston strokes, the kinematic analysis should also provide the estimate of the maximum total discharge necessary to feed all the cylinders. The motion simulators are meant to generate different kinds of motion within a small workspace and study its implication on the payload with high inertia. Therefore, the payload should be excited for any basic motion among SuSwHRPY or a complex motion that combines the basic motions, though roll, pitch and yaw imparted in order. Corresponding to any desired velocity of the platform center of mass and the angular velocity of the platform, the velocity of Points T^i can then be obtained in the stationary coordinate system as

$$\mathbf{v}_{\mathbf{O}(Ti)} = \mathbf{R}_{p,o}^{T}\{\mathbf{v}_{\mathbf{p}(p)} + \boldsymbol{\omega}^{(p)} \times \mathbf{r}_{\mathbf{p}(Ti),(p)}\} \tag{9a}$$

which can be expressed in the corresponding rotating frame as

$$\mathbf{v}_{\mathbf{B}i(Ti)} = (\mathbf{R}_{Bi,o}^{T})^{-1}\, \mathbf{v}_{\mathbf{O}(Ti)} \tag{9b}$$

from which the velocity of the i^{th} piston along its axis can be found out as

$$v_{pi} = \mathbf{v}_{\mathbf{B}i(Ti)}.\hat{k}_{Bi} \tag{9c}$$

yielding the discharges at the top and bottom chambers of each cylinder with flow areas A_t and A_b respectively as

$$q_{ti} = A_t v_{pi} \tag{9d}$$

$$q_{bi} = A_b v_{pi} \tag{9e}$$

The discharges in Equations (9d) and (9e) have been taken as positive and negative respectively for the piston extension and retraction.

Considering the pump and reservoir pressures to be p_p and p_r respectively, a reasonable flow model for most of the commercially available proportional valves [12] has been proposed here with reference to Figure 1 as

$$A_b v_{pi} = \{c_v \max\langle e_i - e_0, 0\rangle + c_l \max\langle \mathrm{sgn}(e_i), 0\rangle\} \mathrm{sgn}(p_p - p_{bi}) \sqrt{|p_p - p_{bi}|} - c_l \max\langle \mathrm{sgn}(e_i), 0\rangle \mathrm{sgn}(p_{bi} - p_r) \sqrt{|p_{bi} - p_r|} + \{c_v \min\langle e_i + e_0, 0\rangle + c_l \min\langle \mathrm{sgn}(e_i), 0\rangle\} \times \mathrm{sgn}(p_{bi} - p_r) \sqrt{|p_{bi} - p_r|} - c_l \min\langle \mathrm{sgn}(e_i), 0\rangle \mathrm{sgn}(p_p - p_{bi}) \sqrt{|p_p - p_{bi}|} \tag{10a}$$

and

$$A_t v_{pi} = \{c_v \max\langle e_i - e_0, 0\rangle + c_l \max\langle \mathrm{sgn}(e_i), 0\rangle\} \mathrm{sgn}(p_{ti} - p_r) \sqrt{|p_{ti} - p_r|} - c_l \max\langle \mathrm{sgn}(e_i), 0\rangle \mathrm{sgn}(p_p - p_{ti}) \sqrt{|p_p - p_{ti}|} + \{c_v \min\langle e_i + e_0, 0\rangle + c_l \min\langle \mathrm{sgn}(e_i), 0\rangle\} \times \mathrm{sgn}(p_p - p_{ti}) \sqrt{|p_p - p_{ti}|} - c_l \min\langle \mathrm{sgn}(e_i), 0\rangle \mathrm{sgn}(p_{ti} - p_r) \sqrt{|p_{ti} - p_r|} \tag{10b}$$

where c_v and c_l are the valve and leakage coefficients, e_i is the command signal to the i^{th} valve, e_0 is the value of a threshold signal and, for ease of appreciation of the use of max and min functions, Figure 1 may be taken up for further discussion, considering the pump and return ports to be metered and the other two ports for communicating the flow between the valve and the cylinder to be unmetered.

At the metered ports, the discharges from the pump and to the reservoir have been indicated in Figure 1 as q_{si} and q_{ri}. The metered ports open or close in pair depending on the command signal, whereas the unmetered ports always remain wide open. Other conditions remaining unchanged, the flow increase in the metered ports is proportional to the increase in the magnitude of the command signal beyond the threshold. The direction of flow in the unmetered ports depends on the sign of the command signal. In order to simulate this direction, the max and min functions have been used in the above two equations. The flow connectivity through these ports has been shown corresponding to the valve at the neutral position and the command-signal dependent swapping of flow directions have been indicated by the two blocks on either side of the neutral block.

The neutral position of the valve is an approximate representation of the system for command signal between the thresholds of $\pm\, e_0$. Within this range of excitation, the flow through the valve is constituted essentially by leakage at each metered port, each of which has two parts. As the piston head divides the cylinder volume in two chambers, the central land of the spool divides the spool in two chambers each extending up to the corresponding end lands. A spool rod connects the three lands providing identical displacement to each by the command signal. At the neutral, the lands completely block the metered ports and the spool movement away from the neutral controls the opening and closing of the metered ports. If the pump flow is metered by the central land by simultaneous covering and uncovering of the port on either side of the land, each end land meters a part of the return ports that are internally connected together within the valve body. In each chamber on either side of the central land, there is also an unmetered port for communicating the main flow with the cylinder.

Beyond the threshold, the increase in the main flow takes place through one part of the pump port and one part of the return port that belong to the opposite chambers. With reversal of sign in the command signal, the parts of the ports with augmented discharge get swapped with respect to the central land. Thus, whether the flow reaches the bottom or top chamber of the cylinder and comes out from the opposite chamber gets decided causing extension or retraction of the piston respectively. The swapping of the main flow paths have been captured by the max and min functions in Equations (10a) and (10b). These equations have been written for a valve with matched and symmetric ports, implying the pump and return ports always opening or closing together in pair by the same amount. The flow model proposed here is more

comprehensive than the one employed in the earlier studies [9, 10]. It is apparent from the above discussion that for positive command signal beyond e_0, the discharge q_{si} that enters a valve chamber from the pump line can be expressed as

$$q_{si} = \{c_v(e_i - e_0) + c_l\}\sqrt{p_p - p_{bi}} + c_l\sqrt{p_p - p_{ti}} \quad (10c)$$

out of which the leakage discharge

$$q_l = c_l(\sqrt{p_p - p_{bi}} + \sqrt{p_p - p_{ti}}) \quad (10d)$$

returns to the reservoir. Of course, prior to flowing through the return port, the latter part of the leakage is joined by the discharge $A_t v_{pi}$ coming from the top chamber of the cylinder. Equations (10c) and (10d) are useful for estimating the coefficients from the given characteristics of a valve.

The inverse kinematic solution of the piston velocities along with Equations (10a) and (10b) provide a system of twelve equations for eighteen unknowns of cylinder pressures and valve command signals. In order to make the system fully deterministic, the inverse dynamic modeling of the system needs to be integrated.

IV. INVERSE DYNAMIC MODELING

The pressure force $F_{B^{iz}}^{ci}$ developed in the i^{th} cylinder along B^{iz} direction by pressurized oil overcoming the friction force F_{fi} and the piston inertia due to the piston mass m_p and acceleration a_{pi} can be expressed as

$$F_{B^{iz}}^{ci} = A_{bi}p_{bi} - A_t p_{ti} - F_{fi} - m_p a_{pi} \quad (11)$$

The cylinder friction is a major source of friction and the system nonlinearity in hydraulic systems. Das et al. [11] developed an easy-to-use model for its complex behavior as shown in fig 3.

All the forces obtained from Equation (11) can be expressed together for later convenience as

$$\mathbf{F}_{\mathbf{B}^z}^{\mathbf{c}} = (F_{B^{1z}}^{c1} \quad F_{B^{2z}}^{c2} \quad F_{B^{3z}}^{c3} \quad F_{B^{4z}}^{c4} \quad F_{B^{5z}}^{c5} \quad F_{B^{6z}}^{c6})^T \quad (12)$$

These forces together support the weight of all the pistons, top joints, disc and payload along with overcoming the inertia of the payload, the disc and the legs. By the choice of the coordinate system, the rotational inertia force $F_{B^{ix}}^{ci}$ of the i^{th} cylinder and piston acts along B^{ix} direction. This force for the i^{th} leg is made of the inertia force on each of the components due to a linear variation of the angular acceleration. Assuming symmetric mass distribution about the principal axes in each component, this force can be calculated as equal to the inertia due to a lumped mass at the mid-point of the axial extent. Therefore, combining the transverse inertia forces in the rotating top arm of the universal joint, the cylinder, the piston and the bottom arm of the spherical joint with lengths l_u, l_c, l_p and l_s respectively and masses m_u, m_c, m_p and m_s respectively, it can be written that

$$F_{B^{ix}}^{ci} = [m_u l_u + m_c(l_u + l_c) + m_p(2l_{ai} - 2l_s - l_p) + m_s(2l_{ai} - l_s)]a_{B^{ix}(Ti)}/(2l_{ai}) \quad (13a)$$

where $a_{B^{ix}(Ti)} = \mathbf{a}_{\mathbf{B}i(Ti)}.\hat{i}_{Bi}$, (13b)

$$\mathbf{a}_{\mathbf{B}i(Ti)} = (\mathbf{R}_{Bi,o}^T)^{-1}\mathbf{a}_{\mathbf{O}(Ti)}, \quad (13c)$$

$$\mathbf{a}_{\mathbf{O}(Ti)} = \mathbf{R}_{p,o}^T\{\mathbf{a}_{\mathbf{p}(p)} + \boldsymbol{\alpha}^{(p)} \times \mathbf{r}_{\mathbf{p}(Ti),(p)} + \boldsymbol{\omega}^{(p)} \times \boldsymbol{\omega}^{(p)} \times \mathbf{r}_{\mathbf{p}(Ti),(p)}\}. \quad (13d)$$

Yet again for later convenience, the forces obtained through Equations (13a) to (13d) for all the legs together are expressed as

$$\mathbf{F}_{\mathbf{B}^x}^{\mathbf{c}} = (F_{B^{1x}}^{c1} \quad F_{B^{2x}}^{c2} \quad F_{B^{3x}}^{c3} \quad F_{B^{4x}}^{c4} \quad F_{B^{5x}}^{c5} \quad F_{B^{6x}}^{c6})^T. \quad (14)$$

Now, representing the third column of the transformation matrix in Equation (5a) as

$$\mathbf{k}_{p,o} = (-c\theta_x s\theta_y c\theta_z + s\theta_x s\theta_z \quad -c\theta_x s\theta_y s\theta_z + s\theta_x c\theta_z \quad c\theta_x c\theta_y)^T \quad (15a)$$

and introducing the compact notations as

$$\mathbf{r}_{(\mathbf{T}),(p)} = \mathbf{R}_{p,o}^T \times (\mathbf{r}_{p^{\mathbf{x}}(T1),(p)} \quad \mathbf{r}_{p^{\mathbf{x}}(T2),(p)} \quad \mathbf{r}_{p^{\mathbf{x}}(T3),(p)} \quad \mathbf{r}_{p^{\mathbf{x}}(T4),(p)} \quad \mathbf{r}_{p^{\mathbf{x}}(T5),(p)} \quad \mathbf{r}_{p^{\mathbf{x}}(T6),(p)}) \quad (15b)$$

$$\mathbf{r}_{B^{\mathbf{ix}}(Ti),(p)} = (r_{B^{ix}(Ti),(p)} \quad r_{B^{iy}(Ti),(p)} \quad r_{B^{iz}(Ti),(p)})^T = (\mathbf{R}_{Bi,o}^{-1})^T \mathbf{r}_{(\mathbf{T}),(p)}(:,i) \quad (15c)$$

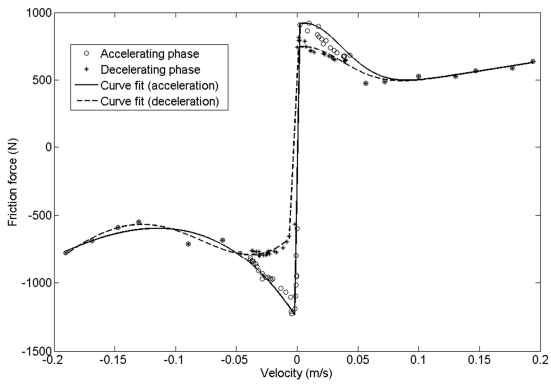

Fig. 2. Typical variation of friction force with piston velocity in a hydraulic cylinder

with(:,*i*) in Equation (16c) representing the i^{th} column of a matrix and $I^{(p)}$ in Equation (16d) representing the mass moment of the moving platform and payload together, the forces on the moving platform imparted through the top joints can be related to linear and angular accelerations of the platform as

$$\mathbf{R}_{p,o}^{T}[\{\begin{pmatrix}\mathbf{i}_{px}^{T}\cdot\sum_{i=1}^{6}\{\mathbf{i}_{Bix}^{T}\mathbf{F}_{\mathbf{B}^{x}(\mathbf{T})}(i) & \mathbf{j}_{px}^{T}\cdot\sum_{i=1}^{6}\{\mathbf{i}_{Bix}^{T}\mathbf{F}_{\mathbf{B}^{x}(\mathbf{T})}(i) & \mathbf{k}_{px}^{T}\cdot\sum_{i=1}^{6}\{\mathbf{i}_{Bix}^{T}\mathbf{F}_{\mathbf{B}^{x}(\mathbf{T})}(i)\\ +\mathbf{k}_{Bix}^{T}\mathbf{F}_{\mathbf{B}^{z}(\mathbf{T})}(i)\} & +\mathbf{k}_{Bix}^{T}\mathbf{F}_{\mathbf{B}^{z}(\mathbf{T})}(i)\} & +\mathbf{k}_{Bix}^{T}\mathbf{F}_{\mathbf{B}^{z}(\mathbf{T})}(i)\}\end{pmatrix}^{T}/m_p\}-g\mathbf{k}_{p,o}]=\mathbf{a} \quad (16a)$$

and

$$[diag(I_{p^x}^{(p)} \quad I_{p^y}^{(p)} \quad I_{p^z}^{(p)})]^{-1}\times[((I_{p^y}^{(p)}-I_{p^z}^{(p)})\omega_{p^y}^{(p)}\omega_{p^z}^{(p)} \quad (I_{p^z}^{(p)}-I_{p^x}^{(p)})\omega_{p^z}^{(p)}\omega_{p^x}^{(p)} \quad (I_{p^x}^{(p)}-I_{p^y}^{(p)})\omega_{p^x}^{(p)}\omega_{p^y}^{(p)})^{T}+$$

$$(\mathbf{R}_{p,o}^{T})^{-1}\begin{Bmatrix}\mathbf{i}_{px}^{T}\cdot\sum_{i=1}^{6}[\mathbf{r}_{(\mathbf{T}),(p)}(:,i)\times\{\mathbf{i}_{Bix}^{T}\mathbf{F}_{\mathbf{B}^{x}(\mathbf{T})}(i)+\mathbf{k}_{Bix}^{T}\mathbf{F}_{\mathbf{B}^{z}(\mathbf{T})}(i)\}]\\ \mathbf{j}_{px}^{T}\cdot\sum_{i=1}^{6}[\mathbf{r}_{(\mathbf{T}),(p)}(:,i)\times\{\mathbf{i}_{Bix}^{T}\mathbf{F}_{\mathbf{B}^{x}(\mathbf{T})}(i)+\mathbf{k}_{Bix}^{T}\mathbf{F}_{\mathbf{B}^{z}(\mathbf{T})}(i)\}]\\ \mathbf{k}_{px}^{T}\cdot\sum_{i=1}^{6}[\mathbf{r}_{(\mathbf{T}),(p)}(:,i)\times\{\mathbf{i}_{Bix}^{T}\mathbf{F}_{\mathbf{B}^{x}(\mathbf{T})}(i)+\mathbf{k}_{Bix}^{T}\mathbf{F}_{\mathbf{B}^{z}(\mathbf{T})}(i)\}]\end{Bmatrix}]=\boldsymbol{\alpha}^{(p)} \quad (16b)$$

Equations (16a) and (16b) can be solved together for the six unknowns represented by the right-hand side of Equation (12) with the forces in Equation (14) obtained for any choice of the motion profile of the payload that also defines the right-hand side vector in Equations (16a) and (16b). Equations (10a), (10b) and (11) can then be solved together at any instant of time to obtain the cylinder pressures and the command signal. Thus the inverse kinematic and dynamic models can be employed together for designing the system.

V. Design through Numerical Simulation

In order to accomplish the design analysis, the formulation presented above has been implemented in Matlab-Simulink framework. Prior to the implementation, the valve and leakage coefficients of the proportional valves need to be ascertained from the known characteristics of available commercial valves. Along with the characteristics, any such valve has specifications for the maximum discharge and the maximum leakage expressed as *p*% of the maximum discharge. From Equations (10c) and (10d) with equal pressure drop Δp in each metered port, it can thus be written that $c_l = pc_v(e_{\max}-e_0)/(200-2p)$ that along with Equation (10c) provides

$$q_{si}=\{e_i-e_0+p(e_{\max}-e_0)/(200-2p)\}c_v\sqrt{\Delta p_v/2}+\{p(e_{\max}-e_0)c_v\sqrt{\Delta p_v/2}\}/(200-2p) \quad (17)$$

where Δp_v is the total pressure drop in the two metered ports.

VI. Results

Theoretical result of the mathematical model described is prepared using a programming in MATLAB under the following specifications of the geometric and dynamic parameters of the model.

$r_b = 0.5m$

$r_t = 0.3m$

$z_{(q)}^{0} = 0.9m$

Arm length of each joint (top and bottom) $= t_iT_i = b_iB_i$ =0.1m

Mass of pay load(m_{pay}) = 250kg, radius of pay load(r_{pay})=0.15m, density((ρ_{pay}) =7900kg/m^3

Mass of steel plate +Mass of hexagonal frame=60kg+30kg=90kg.

Maximum displacement from neutral position along x direction (surge motion) =0.05m $\rangle x$

Maximum displacement from neutral position along y direction (sway motion) = 0.05m $\rangle y$

Maximum displacement from neutral position along z direction (heave motion) =0.15m $\rangle z$

Maximum linear velocity ($\mathbf{v_{max}}$) =0.3m/s, Linear acceleration/retardation (**a**) =3m/s^2.

Maximum angular velocity ($\omega_{\max}$) = $20^0/s$, Angular acceleration/retardation (α) = $200^0/s^2$

A required table movement is given in such a way that initially accelerated up to the maximum velocity then at constant velocity $\mathbf{v_{max}}$ then retarded to rest at the final position based on the above specification force requirement on each actuator for different table movement is found out as shown in fig 5a & 5b. Analyzing the above force variation for different table movements, lower series of cylinder piston assembly from Bosch Rexroth catalog is selected

Cylinder diameter = 0.025m and Piston diameter = 0.012m.Maximum pressure (P_s) generated by the pump is selected as 50bar. Considering loss of flow rate in % (p) =20. Block diagram of the hydraulic circuit is shown in fig 1.

Calculation of C_V

Arbitrarily sample points are chosen from the

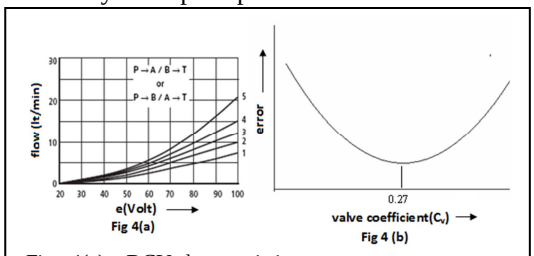

Fig. 4(a) DCV characteristic curve
Fig 4(b) Error variation with valve coefficient

characteristic curve as shown in Fig (4a) of the DCV

which are tabulated in a table for different pressure & % opening in terms of voltage, flow rates in lt/min are extracted. From these data a rough calculation suggests that average value of C_v should be in the range between 0.1 & 0.35. For each of these C_v flow rate is calculated using the equation (10). After that an error parameter

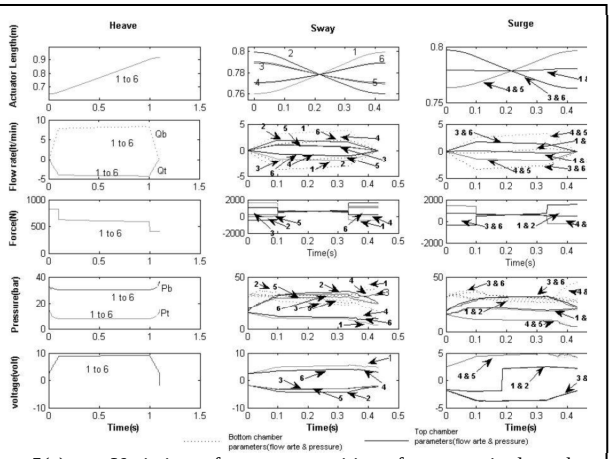

Fig. 5(a) Variation of actuator position, force required at the actuators along the actuators, flow rate supplied at the top & bottom chamber, pressure required at the top & bottom chamber & voltage required to control the opening of the valve during the motion with respect to time is plotted for heave, sway & surge motion.

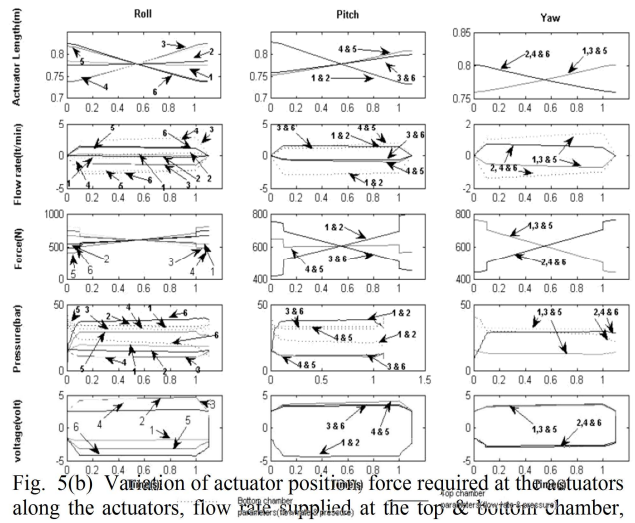

Fig. 5(b) Variation of actuator positions force required at the actuators along the actuators, flow rate supplied at the top & bottom chamber, pressure required at the top & bottom chamber & voltage required to control the opening of the valve during the motion with respect to time is plotted for roll, pitch & yaw motion.

$e = \sum (Q_{graph} - Q_{calculated})^2$ is calculated for each C_v and least value of error corresponding to C_v=0.27 is taken as the valve coefficient. Variation of error with C_v is shown in Fig (4b).

Now solving equations 10a, 10b, 14 and 11 for different types of specified motion flow rate variation into the actuator(positive) or coming out from the actuator(negative), pressure variation in top and bottom chamber of each actuator and the instantaneous valve openings are plotted with time in fig5a & fig5b.

It can be concluded for the above mentioned basic motions maximum flow that the pump is required to supply is 49.91 lt/min during heave motion.

VII. CONCLUSIONS

A simple discharge model for commercial valves has been proposed and the methodology for determining its various coefficients has been demonstrated. The usefulness of a simple friction model developed by Das et al. [11] has been clearly brought out in designing a system as complex as a Stewart platform. In fact the complete methodology provided for designing such a system prior to designing the controls is a notable contribution of the present study. The inverse models for the system kinematics and dynamics have been used in Matlab for accomplishing the design. The margins left in the valve command signals need to be tested for the control analysis as one described by Halder et al. [2].

ACKNOWLEDGMENT

We sincerely acknowledge RCI Hyderabad, India for providing us with the scholarship support. In particular, we express our gratefulness to Mr. S. K. Roy, Director RCI, Mr. J. P. Singh, Scientist RCI and Late Mr. P. Banerjee, Former Director Eliora Hyderabad.

REFERENCES

[1] D. Stewart, A platform with six degrees of freedom, Proceedings of Institute of Mechanical Engineering 180 (1) (1965) 371–386.

[2] B. Halder, R. Saha, D. Sanyal, Control-integrated design by theoretical simulation for a torque-actuated 6-SBU Stewart platform, AMAE Int. J. on Manufacturing and Material Science, 2(1), (2012), 13-21.

[3] K. Liu, J. Fitzgerald, F. L. Lewis, Kinematic analysis of a Stewart platform manipulator, IEEE Transactions on Industrial Electronics, 40 (2) 1993) 282–293.

[4] J. -P. Merlet, Direct kinematics of parallel manipulators, IEEE Transactions on Robotics and Automation, 9 (6) (1993) 842-845.

[5] B. Dasgupta, T. S. Mruthyunjaya, Closed-form dynamic equations of the general Stewart platform through the Newton–Euler approach, Mechanisms and Machines Theory 33 (7) (1998) 993–1012.

[6] B. Dasgupta, T. S. Mruthyunjaya, A Newton–Euler formulation for the inverse dynamics of the Stewart platform manipulator, Mechanisms and Machines Theory 33 (7) (1998) 1135–1152.

[7] C. I. Huang, C. F. Chang, M. Y. Yu and L. C. Fu, Sliding-Mode tracking control of the Stewart platform, 5th Asian Control Conference (2004) 561-568.

[8] C. I. Huang and L. C. Fu, Smooth sliding-Mode tracking control of the Stewart platform, Proceedings of the 2005 IEEE Conference on Control Applications (2005) 561-568.

[9] D. Li, S.E. Salcudean, Modeling simulation and control of a hydraulic stewart platform, Proceedings of the IEEE International Conference on Robotics and Automation (1997) 3360–3366.

[10] I. Davliakos, E. Papadopoulos, Model-based control of a 6-dof electrohydraulic Stewart–Gough platform, Mechanism and Machine Theory 43 (2008) 1385–1400.

[11] Sarkar BK, Das J, Saha R, Mookherjee S and Sanyal D. Approaching servoclass tracking performance by a proportional valve-controlled system, IEEE/ASME Trans. on Mechatronics (2013) 1425–1430.

[12] Engineering Mannesman-Rexroth Catalogue, 4/2 and 4/3 proportional directional valves directly controlled, with electrical position feedback Types 4WRE and 4WREE, RE 29 061/09, 2009.